RESEARCH ARTICLE

CrossMark

Quantitative mechanisms of cadmium adsorption on rice straw- and swine manure-derived biochars

Yiyi Deng[1] · Shuang Huang[1] · David A. Laird[2] · Xiugui Wang[1] · Caiqin Dong[1]

Abstract

We quantified and investigated mechanisms for Cd^{2+} adsorption on biochars produced from plant residual and animal waste at various temperatures. Ten biochars were produced by pyrolysis of rice straw (RB) and swine manure (SB) at 300–700 °C and characterized. The Cd^{2+} adsorption isotherms, adsorption kinetics, and desorption characteristics were studied via a series of batch experiments, and Cd^{2+}-loaded biochars were analyzed by SEM–EDS and XRD. The total Cd^{2+} adsorption capacity (Q_c) increased with pyrolysis temperature for both biochars, however, rice straw-derived biochars had greater Q_c than swine manure-derived biochars; hence, the biochar derived from rice straw at 700 °C (RB700) had the largest Q_c, 64.4 mg g^{-1}, of all studied biochars. Cadmium adsorption mechanisms in this study involved precipitation with minerals (Q_{cp}), cation exchange (Q_{ci}), complexation with surface functional groups (Q_{co}), and Cd-π interactions ($Q_{c\pi}$). Both the pyrolysis temperature and feedstock affected the quantitative contributions of the various adsorption mechanisms. The relative percent contributions to Q_c for Cd^{2+} adsorption by RB and SB were 32.9–72.9% and 35.0–72.5% for Q_{cp}, 21.7–50.9% and 20.4–43.3% for Q_{ci}, 2.2–14.8% and 1.4–18.8% for Q_{co}, and 1.4–3.1% and 3.0–5.8% for $Q_{c\pi}$, respectively. For biochars produced at higher pyrolysis temperatures, the contributions of Q_{cp} and $Q_{c\pi}$ to adsorption increased, while the contributions of Q_{ci} and Q_{co} decreased. Generally, Q_{cp} dominated Cd^{2+} adsorption by high-temperature biochars (700 °C) (accounting for approximately 73% of Q_c), and Q_{ci} was the most prominent mechanism for low-temperature biochars (400 °C) (accounting for 43.3–50.9% of Q_c). Results suggested that biochar derived from rice straw is a promising adsorbent for the Cd^{2+} removal from wastewater and that the low-temperature biochars may outperform the high-temperature biochars for Cd^{2+} immobilization in acidic water or soils.

Keywords Biochar · Cadmium · Adsorption mechanism · Desorption · Pyrolysis

✉ Shuang Huang
hsh5527@whu.edu.cn

Yiyi Deng
dyy7076@whu.edu.cn

[1] State Key Laboratory of Water Resources and Hydropower Engineering Science, Wuhan University, Wuhan 430072, China

[2] Department of Agronomy, Iowa State University, Ames, IA 50011, USA

Introduction

In China, pollution of the soil with cadmium (Cd) has become a serious problem. In 2014, the National Survey of Soil Pollution reported that 7.0% of agricultural land was contaminated with Cd above safe levels (Ministry of Environmental Protection and Ministry of Land and Resources 2014). Furthermore, Cd is a trace element with recalcitrance and high mobility in soil and facile accumulation in plants, thus posing a threat to human health via the food chain (Rafiq et al. 2014). Adsorption is an important component of most remediation techniques (Ali and Gupta 2007; Li et al. 2018). Recently, biochar has attracted widespread attention as a new adsorbent for remediation of Cd-contaminated soil and water due to its widespread availability, low cost, high efficiency, and environmental friendliness (Ahmad et al. 2014).

Biochar, a highly stable carbon-rich product, is produced from the pyrolysis of various organic waste materials in the absence of oxygen (Beesley et al. 2011; Ma et al. 2017; Mohammadi et al. 2011). Numerous types of waste biomasses have been used to produce biochar for removing Cd from aqueous solutions and soils (Ahmad et al. 2014; Peng et al. 2017; Wang et al. 2017; Xu et al. 2013a). Plant-derived biochars such as rape straw, rice straw, corn straw, and wheat straw are effective sorbents for Cd removal in aqueous solutions and soils (Bashir et al. 2018; Wang et al. 2018; Xu et al. 2014; Xu et al. 2013a). Manure-derived biochars, including biochars produced from broiler litter, swine manure, and diary manure, can also immobilize Cd in water and soil (Meng et al. 2014; Uchimiya et al. 2010; Xu et al. 2013b). Among these materials, rice straw and swine manure are attractive raw materials for the biochar production considering widespread availability and low cost of the feedstock and high efficiency of the resulting biochar. The improper disposal of rice straw and swine manure (such as open-field burning of rice straw) is a waste of biomass resources and may cause air pollution and eutrophication of water resources. Thus, the production and land application of rice straw- and swine manure-derived biochars are a means of waste resources recovery.

Cadmium removal efficiency and mechanisms of removal by biochar have been previously studied by several researchers. For example, Liu and Fan (2018) studied mechanisms for the removal of Cd from aqueous solutions by wheat straw biochar. Zhang et al. (2015) investigated the efficiency and mechanisms of Cd adsorption by biochars produced from water hyacinth at 250–550 °C. Cui et al. (2016) investigated the Cd adsorption mechanisms by biochars produced from *Canna indica* at 300–600 °C and their quantitative contributions. Potential mechanisms for Cd adsorption onto biochars include the following: (i) precipitation with minerals (e.g., CO_3^{2-}, PO_4^{3-}); cation exchange with metals (e.g., Ca^{2+}, Mg^{2+}, K^+, and Na^+); (iii) surface complexation with oxygen-containing functional groups (OFGs) (e.g., –OH, −R–OH, –COOH); and (iv) interaction with π electrons (e.g., C=C) (Bashir et al. 2018; Chen et al. 2018; Wang et al. 2015; Zhang et al. 2015). The Cd adsorption mechanisms largely depend on properties of the biochars and the solution, such as pH, ionic concentration, and surface characteristics, which are influenced by feedstocks, production conditions, and adsorption conditions (Han et al. 2017; Higashikawa et al. 2016). Many studies have investigated the relationship between biochar properties and Cd^{2+} adsorption based on different pyrolysis production temperatures (Uchimiya et al. 2011; Zhang et al. 2013). However, limited studies have provided systematic and quantitative information on the contributions of different mechanisms to Cd^{2+} adsorption by both plant- and manure-derived biochars prepared at different temperatures. Therefore, because rice straw and swine manure are important feedstocks for biochar production, a systematic and

quantitative investigation of Cd sorption mechanisms by biochars produced from these feedstocks is needed.

Biochars produced at low temperature have more oxygen-containing functional groups and higher CEC (cation exchange capacity), whereas high-temperature biochars have more complete π-conjugated aromatic structures and higher AEC (anion exchange capacity) (Keiluweit et al. 2010; Lawrinenko and Laird 2015; Wang et al. 2015). With increasing pyrolysis temperature, the ash content of biochars increases forming various soluble and insoluble mineral phases (e.g., quartz, carbonates, whitlockite, and calcium silicate), particularly above 500 °C (Fidel et al. 2017; Cao and Harris 2010). Thus, it is reasonable to hypothesize that biochars derived from plant residual and animal waste at various temperatures have different capacities and contributions of mechanisms to Cd^{2+} adsorption.

In this study, the specific objectives were as follows: (1) to investigate the influences of pyrolysis temperature and feedstock on biochar properties and Cd^{2+} adsorption capacity; (2) to identify the optimum biochar type for Cd^{2+} removal from aqueous systems; (3) to determine the characteristics of Cd^{2+} adsorption and desorption for biochars derived from plant and animal waste; and (4) to quantify the contributions of precipitation, cation exchange, surface complexation, and Cd^{2+}-π interactions to the overall Cd^{2+} adsorption by plant- and manure-derived biochars.

Materials and methods

Production of biochars

Rice straw was collected from the Irrigation and Drainage and Water Environment Integrated Experimental Station of Wuhan University, rinsed with tap water three times, and air-dried. Fresh, wet swine manure was obtained from a commercial swine farm in Huangpi City of Hubei Province and air-dried for 2 weeks. Both the air-dried rice straw and swine manure were crushed, ground, and sieved to < 0.3 mm. The sieved biomass feedstocks (40–45 g) were compacted into corundum crucibles (Φ 60 mm × 100 mm) with covers, sealed with tin foil and pyrolyzed at 300, 400, 500, 600, or 700 °C under oxygen-limiting conditions in a muffle furnace. The furnace was heated at a rate of 15 °C per minute and held at the peak temperature for 4 h before cooling to room temperature. The pyrolyzed samples were sealed in airtight containers and labeled according to feedstock and pyrolysis temperature (RBX or SBX, where RB and SB represent rice straw and swine manure biochars, and X represents the peak pyrolysis temperature).

To quantify the contribution of precipitation with minerals to cadmium adsorption onto biochars, biochars were washed with 0.1 mol L^{-1} HCl (50 g biochar L^{-1}) by constant stirring at

200 rpm in a digital water bath oscillator at 25 °C for 1 h; the procedure was repeated three times. Then, the treated biochars were rinsed with deionized water and filtered through 0.45-μm filters several times until the pH of the filtrate was constant. After, the acid-treated biochar samples were dried overnight at 80 °C and labeled ARBX and ASBX (where A indicates acid washed, RB and SB represent rice straw and swine manure biochars, and X represents the pyrolysis temperature).

Characterization of biochars

The following physicochemical properties of the biochars were analyzed: yield, proximate analysis (ash, moisture, VM, and fixed carbon), pH (1:20 water extraction), and EC (electricity conductivity) (1:100 water extraction). The specific surface area (SSA) was measured via N_2 adsorption using an ASAP-2020M analyzer (Micromeritics Instrument Corp., NoRBross, GA, USA). The surface area of the biochars was calculated by fitting the data to the BET equation. The elemental composition (C, H, N, and O) was determined by dry combustion using a Vario EL cube CHNS/O analyzer (Elementar Analyse system GmbH, Hanau, Germany). The functional groups were identified by Fourier transform infrared spectroscopy (FTIR) (Thermo Nicolet Corporation, Waltham, MA, USA). The surface microstructure and morphology were visualized by scanning electron microscopy (SEM) (Carl Zeiss, SIGMA, England). X-ray diffraction (XRD) was conducted using a computer-controlled diffractometer equipped with a stepping motor and a graphite crystal monochromator (PANalytical B.V., Netherlands). Concentrations of Cd^{2+} in solutions were analyzed using an atomic absorption spectrometer (Agilent 240 Duo AA, USA).

Batch experiments

Cd^{2+} stock solutions (1000 mg L^{-1}) were prepared by dissolving Cd $(NO_3)_2 \cdot 4H_2O$ in a 0.005 mol L^{-1} $CaCl_2$ background solution. The adsorption of Cd^{2+} by the rice straw- and swine manure-derived biochars prepared at five temperatures was tested to determine the optimal carbonization temperature using an initial Cd^{2+} solution concentration of 100 mg L^{-1}. In the experiment, 0.02 g biochar was added to 20 mL Cd^{2+} solution with an initial pH value of 5.5 ± 0.1 adjusted by 0.1 M NaOH or HNO_3 and shaken in a digital water bath oscillator at 200 rpm and 25 ± 1 °C for 24 h. A control without Cd^{2+} was prepared under the same conditions. After equilibration, the final pH value of the filtrate was measured. Adsorption isotherms for the RB700 and SB700 biochars were obtained under the same conditions except that the initial concentrations of Cd^{2+} in the solutions were 0, 10, 30, 50, 100, 200, and 400 mg L^{-1}. The kinetics of the adsorption processes were measured for RB700 and SB700 as follows: 20 mL of the

working Cd^{2+} solution (100 mg L^{-1}) was added to 0.02 g of biochar in a 50-mL plastic centrifuge tube, and the tube was shaken in a digital water bath oscillator at 25 ± 1 °C for 0, 5, 10, 30, 60, 90, 120, 240, 480, 720, 1440, or 2880 min. A total of 36 samples, corresponding to 12 times and 3 replicates, were collected. Batch desorption kinetics studies were performed using consecutive adsorption–desorption processes to examine desorption mechanisms. To do so, 36 samples were equilibrated with the 100 mg L^{-1} Cd^{2+} solution for 24 h, then the supernatant was removed by centrifugation. A 20 mL volume of 0.005 mol L^{-1} $CaCl_2$ solution was added to the 50-mL plastic centrifuge tube containing the biochar, and the tube was shaken in a digital water bath oscillator at 25 ± 1 °C for 0, 5, 10, 30, 60, 90, 120, 240, 360, 720, 1440, and 2880 min. Samples were collected at each time and examined. For these experiments, the final suspensions were centrifuged for 20 min at 4000 rpm and filtered through a 0.45-μm syringe filter, and Cd^{2+} concentrations of the filtrates were determined by flame atomic absorption spectrometry (Agilent 240 Duo AA, USA).

To calculate the contribution of each mechanism to the total amount of Cd^{2+} absorbed on biochars, the original and acidified biochars were mixed with Cd^{2+} solution (100 mg L^{-1}) or background solution (control) under the same conditions mentioned previously. The pH values of the samples were measured before and after equilibration. After filtering the samples through a 0.45-μm syringe filter, the concentrations of Ca^{2+}, Mg^{2+}, K^+, and Na^+ were analyzed using ICP-MS (Perkin Elmer Ltd., USA), and the Cd^{2+}-loaded biochars were collected for XRD and SEM-EDS analyses.

The amounts of Cd^{2+} absorbed (Q_t) were calculated according to;

$$Q_t = \frac{(C_0 - C_t)V}{m} \tag{1}$$

where Q_t (mg g^{-1}) is the amount of Cd^{2+} absorbed at time t, C_0 (mg L^{-1}) and C_t (mg L^{-1}) are the initial Cd^{2+} concentration and the Cd^{2+} concentration at time t, respectively, V (L) is the volume of solution, and m (g) is the mass of biochar.

The isotherm data for Cd^{2+} adsorption onto biochars was fitted by the Langmuir (Eq. (2)) and Freundlich (Eq. (3)) models:

$$Q_e = \frac{Q_m K_L C_e}{1 + K_L C_e} \tag{2}$$

$$Q_e = K_F C_e{}^n \tag{3}$$

where C_e (mg L^{-1}) is the equilibrium concentration of Cd^{2+} in aqueous solution, Q_e (mg g^{-1}) is the amount of Cd^{2+} adsorbed onto the biochar at equilibrium, Q_m (mg g^{-1}) is the maximum adsorption capacity of the biochar, K_L (L mg^{-1}) is the adsorption coefficient of Langmuir model, K_F (mg g^{-1}) (mg L^{-1})$^{-n}$ is

the adsorption coefficient of Freundlich model, and n (dimensionless) is the adsorption constant of the Freundlich model related to the surface site heterogeneity.

The kinetics of Cd^{2+} adsorption on biochars were fitted by a pseudo-first-order equation (PFO model, Eq. (4)), a pseudo-second-order equation (PSO model, Eq. (5)), the Elovich equation (Eq. (6)), the intraparticle diffusion equation (IPD model, Eq. (7)), and a two-compartment model (TC model, Eq. (8)), which can be presented as follows:

$$Q_t = Q_e\left(1 - e^{-k_1 t}\right) \tag{4}$$

$$Q_t = \frac{k_2 Q_e^{2} t}{1 + k_2 Q_e t} \tag{5}$$

$$Q_t = \frac{1}{\beta}\ln(t) + \frac{1}{\beta}\ln(\alpha\beta) \tag{6}$$

$$Q_t = k_p \sqrt{t} + b \tag{7}$$

$$\frac{Q_t}{Q_e} = 1 - \left(F_{fast} e^{-k_{fast} t} + F_{slow} e^{-k_{slow} t}\right) \tag{8}$$

where k_1 (h^{-1}) is the rate constant of the pseudo-first-order equation, k_2 ($g\ mg^{-1}\ h^{-1}$) is the rate constant of the pseudo-second-order equation, α ($mg\ g^{-1}\ h^{-1}$) is the initial adsorption rate constant of the Elovich model, β ($g\ mg^{-1}$) is a parameter related to the extent of surface coverage and activation energy for chemisorption, k_p ($mg\ g^{-1}\ h^{-0.5}$) is the rate constant of intraparticle diffusion, b ($mg\ g^{-1}$) is the intercept, and F_{fast} and F_{slow} are the mass fractions ($F_{fast} + F_{slow} = 1$), and k_{fast} (h^{-1}) and k_{slow} (h^{-1}) are the first-order rate constants for the adsorbent transporting into the "fast" and "slow" compartments, respectively.

Quantitative contributions of Cd^{2+} adsorption mechanisms

The contributions of Cd^{2+} adsorption mechanisms by biochars were determined using the method proposed by Wang et al. (2015) and further modified by Cui et al. (2016). The Cd^{2+} adsorption capacity attributed to cation exchange (Q_{ci}), precipitation with minerals (Q_{cp}), oxygen-containing functional group complexation (Q_{co}), and Cd^{2+}-π interaction ($Q_{c\pi}$) were calculated. Other potential mechanisms caused by clay minerals and oxides (e.g., Al/Fe/Mn–OH + M → Al/Fe/Mn–O–M + H) were neglected in the study.

(i)   The contribution of interaction with minerals to Cd^{2+} adsorption (Q_{cm}) was calculated as follows:

$$Q_{cm} = Q_c - Q_a \tag{9}$$

where Q_{cm} ($mg\ g^{-1}$) is the amount of Cd^{2+} adsorbed due to interaction with minerals, Q_c ($mg\ g^{-1}$) is the total amount of Cd^{2+} adsorbed onto biochars, and Q_a ($mg\ g^{-1}$) is the amount of Cd^{2+} adsorbed by the acidified biochars.

(ii)   The absorbed amounts of Cd^{2+} resulting from cation exchange (Q_{ci}) was calculated by the difference in the concentrations of the metal cations (Ca^{2+}, Mg^{2+}, K^+, and Na^+) in solution before and after Cd^{2+} adsorption.

$$Q_{ci} = Q_{Ca} + Q_{Mg} + Q_K + Q_{Na} \tag{10}$$

where Q_{Ca}, Q_{Mg}, Q_K, and Q_{Na}, are the net amounts of Ca^{2+}, Mg^{2+}, K^+, and Na^+ released from the biochars to solution after the Cd^{2+} adsorption, respectively, in milliequivalents per liter.

(iii)   The effects of minerals on Cd^{2+} adsorption are attributed to both the cation exchange and precipitation with mineral, thus the contribution of precipitation with minerals to Cd^{2+} adsorption (Q_{cp}) can be defined as the difference between Q_{cm} and Q_{ci}.

$$Q_{cp} = Q_{cm} - Q_{ci} \tag{11}$$

(iv)   The reactions of Cd^{2+} with oxygen-containing functional groups can be described as follows (Cao et al. 2009):

$$-COOH + Cd^{2+} + H_2O \rightarrow -COOCd^+ + H_3O^+ \tag{12}$$

$$-OH + Cd^{2+} + H_2O \rightarrow -OCd^+ + H_3O^+ \tag{13}$$
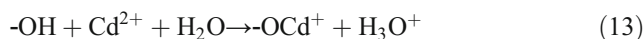
The Cd^{2+} adsorption caused by the oxygen-containing functional groups' complexation (Q_{co}) was determined by the amount of H^+ released or the drop in pH after the Cd^{2+} adsorption onto acidified biochars.

(v)   The amount of Cd^{2+} adsorbed through Cd^{2+}-π interactions ($Q_{c\pi}$) was calculated as follows:

$$Q_{c\pi} = Q_a - Q_{co} \tag{14}$$

The proportions of different mechanisms to the Cd^{2+} adsorption were defined by the ratios Q_{ci}/Q_c, Q_{cp}/Q_c, Q_{co}/Q_c, and $Q_{c\pi}/Q_c$.

Statistical analysis

In this study, the batch experiments of Cd^{2+} adsorption were performed using triplicate samples, and the other experimental data were obtained from duplicate samples, except for some

with specific notes. The means, standard deviations, and regression correlation coefficients were computed using Microsoft 2010 Excel software. Significant differences were tested after analysis of variance using Duncan's multiple range test ($p = 0.05$) by SPSS 19.0. The kinetics and adsorption isotherms were fitted using Origin 9.0.

Results and discussions

Characterization of biochars

Table 1 provides the yield, ash, moisture, proximate analysis, pH, EC, and specific surface area of the rice straw- and swine manure-derived biochars produced at 300–700 °C. The biochar yield decreases as the pyrolysis temperature increased from 300 to 700 °C and the yield of RB was higher than that of SB. For all biochars considered, the ash content of RB and SB significantly increased with increasing pyrolysis temperature, and the highest ash content, 52.6%, was observed for SB700. As pyrolysis temperature increased from 300 to 700 °C, the contents of volatile matters (VM) of RB and SB decreased from 36.36 to 13.01% and from 40.35 to 13.71%, respectively. The fixed carbon content of RB was higher than that of SB for 300–700 °C. The differences in the VM and fixed carbon contents between RB and SB probably resulted from differences in the composition of the feedstocks; rice straw is rich in cellulose and hemicellulose, and swine manure contains more protein and organic acids (Shinogi and Kanri 2003; Uchimiya et al. 2011). Between 300 and 500 °C, the specific surface areas (SSA) of RB and SB increased relatively slowly from 3.05 to 7.67 m^2 g^{-1} and from 2.27 to 9.70 m^2 g^{-1}, respectively. When the pyrolysis temperature increased to 600 °C, the SSA increased sharply, reaching 16.38 m^2 g^{-1} and 99.01 m^2 g^{-1}, respectively. The rapid release of the VM at 500–600 °C led to the extensive formation of voids (Shinogi and Kanri 2003).

pH is an indicator of biochar ash composition and surface properties (Fidel et al. 2017; Yuan et al. 2011). As pyrolysis temperature increased from 300 to 400 °C, the pH of RB and SB increased from 9.04 to 10.22 and from 8.31 to 10.34, respectively. Increases in pH with pyrolysis temperature can be explained by the formation of alkali and alkaline earth carbonates and by the evaporation of the acidic substances during the pyrolysis process (Cao and Harris 2010; Pan et al. 2013; Shinogi and Kanri 2003). The biochar electrical conductivity (EC) values varied from 175 to 1137 μS cm^{-1}. RB showed larger EC values than SB at each temperature, implying that RB is typically high in EC-influencing elements.

Elemental analysis (C, H, N, and O) showed that C was the primary element in RB and SB, and the ratios of H, N, and O to C decreased with increasing pyrolysis temperature (Table 1). The aromaticity and polarity of chars are usually estimated by the atomic ratios of elements (H/C and O/C and (O+N)/C, respectively), due to the removal of polar functional groups and formation of aromatic structures by the carbonization of organic materials during pyrolysis (Chen et al. 2008; Uchimiya et al. 2011). In this study, the H/C ratios of RB and SB decreased from 1.7 before pyrolysis to below 0.5 at 500–700 °C, indicating that the aromaticity of RB and SB increased with increasing temperature. The lower (N+O)/C ratios of RB indicated that fewer polar functional groups were on the surfaces of RB relative to SB produced at the same temperature.

Surface morphology, chemical functional groups, and the crystalline state of minerals on the biochars' (RB and SB) surface were characterized by SEM (Fig. S1 and Fig. S2 for RB and SB, respectively), FTIR (Fig. S3), and XRD (Fig. S4).

Impacts of pyrolysis temperature and feedstock on Cd^{2+} adsorption capacity of biochar

Figure 1a shows the Cd^{2+} adsorption capacities for the RB and SB produced at 300 to 700 °C in solution with an initial Cd^{2+} concentration of 100 mg L^{-1}. The Cd^{2+} adsorption capacities of RB and SB increased with pyrolysis temperature, with the adsorption capacities of 64.4 mg g^{-1} and 34.2 mg g^{-1}, respectively. Based on a single factor analysis of variance (Fig. 1a), there were significant differences among the Cd^{2+} adsorption capacities of rice straw- and swine manure-derived biochars produced at all pyrolysis temperatures; thus, 700 °C is the optimal production temperature for removing Cd^{2+} from aqueous solutions. A previous study reported that an increase in the Cd^{2+} adsorption capacity of a biochar with pyrolysis temperature was related to an increase in surface area and the development of micropores with condensation of aromatic carbon (Keiluweit et al. 2010). Lee et al. (2015) reported that 800 °C was the most effective pyrolysis temperature for preparing peat moss biochars to remove heavy metals (Cu, Pb, and Cd), and claimed that an increase in pH at higher temperatures increased the amount of negative charges on the surface of the adsorbent. Chen et al. (2014) studied urban sewage sludge biochars prepared at 500–900 °C and found the Cd adsorption increased with pyrolysis temperature due to the increased porosity in the biochars. This proposed mechanism, however, conflicts with evidence from other reports that negative surface charge and CEC decrease with increasing pyrolysis temperature (Banik et al. 2018; Lawrinenko and Laird 2015). Han et al. (2017) found that Cd^{2+} adsorption capacity of biochars derived from swine solids and poultry litter decreased with increased pyrolysis temperature (250–600 °C), and Zhang et al. (2015) reported that Cd^{2+} adsorption capacity of water hyacinth-derived biochar produced at 450 °C outperformed the other biochars (produced at 250–550 °C). These inconsistent influences of pyrolysis temperature on Cd adsorption of biochars could result from feedstock type

Table 1 Properties of rice straw and swine manure biochars produced at 300–700 °C

Biochar	Yield [a] (wt.%)	pH [a]	EC [b] ($\mu S\ cm^{-1}$)	SSA [a] ($m^2\ g^{-1}$)	Proximate analysis (wt.%db)				Elemental content (wt.%db)				Atomic ratio		
					Moisture [b]	VM [b]	Ash [b]	Fixed C [c]	C	H	O	N	H/C	O/C	(O+N)/C
RB300	47.62 ± 0.08	9.04 ± 0.07	1137 ± 3.54	3.05 ± 1.27	2.49 ± 0.05	36.36 ± 0.05	30.19 ± 0.25	30.96	45.10	3.38	27.79	1.81	0.90	0.46	0.50
RB400	38.75 ± 0.02	10.22 ± 0.01	779 ± 2.73	3.97 ± 1.40	2.27 ± 0.03	26.09 ± 0.03	32.28 ± 0.51	39.36	43.03	1.82	24.96	1.55	0.51	0.44	0.47
RB500	34.77 ± 0.01	10.30 ± 0.02	973 ± 1.41	7.67 ± 2.01	1.69 ± 0.05	18.97 ± 0.05	33.04 ± 0.87	46.30	44.31	0.91	23.57	1.47	0.25	0.40	0.43
RB600	32.21 ± 0.01	10.34 ± 0.01	672 ± 6.87	16.38 ± 1.87	1.79 ± 0.03	15.63 ± 0.03	34.19 ± 0.01	48.40	45.86	0.34	22.78	0.94	0.09	0.37	0.39
RB700	30.51 ± 0.05	10.58 ± 0.05	691 ± 4.95	29.06 ± 3.64	1.44 ± 0.02	13.01 ± 0.02	40.91 ± 0.80	44.65	43.64	0.00	20.35	1.05	0.00	0.35	0.37
SB300	53.64 ± 0.04	8.31 ± 0.09	425 ± 1.41	2.27 ± 1.07	2.16 ± 0.03	40.35 ± 0.06	31.61 ± 0.75	25.88	37.43	3.40	26.87	3.86	1.09	0.54	0.63
SB400	42.99 ± 0.03	10.34 ± 0.03	457 ± 3.44	2.40 ± 0.98	2.07 ± 0.17	29.17 ± 0.04	34.51 ± 0.89	34.25	38.58	1.77	26.57	3.12	0.55	0.52	0.59
SB500	39.46 ± 0.02	10.24 ± 0.02	442 ± 5.46	9.70 ± 1.35	1.30 ± 0.01	19.42 ± 0.01	41.30 ± 0.76	37.97	39.62	0.29	25.14	2.82	0.09	0.48	0.54
SB600	36.41 ± 0.01	10.78 ± 0.02	219 ± 9.19	99.01 ± 12.46	1.42 ± 0.14	16.56 ± 0.02	48.11 ± 0.33	33.91	37.62	0.16	23.49	2.28	0.05	0.47	0.52
SB700	35.98 ± 0.01	10.58 ± 0.06	175 ± 2.97	163.01 ± 9.86	0.97 ± 0.23	13.71 ± 0.01	52.80 ± 0.50	32.51	40.97	0.00	22.01	1.74	0.00	0.40	0.44

[a] Mean ± SD for replicate production

[b] Proximate analysis results are given as the mean ± SD for duplicate measurements

[c] Calculated by difference after moisture, VM and ash measurement

db Oven-dry basis

effects, which have more influences on the Cd adsorption than temperatures (Higashikawa et al. 2016).

As shown in Fig. 1a, the Cd^{2+} adsorption capacity of RB was larger than that of SB at a given temperature (300–700 °C). The result suggested that rice straw-derived biochars were more effective for Cd^{2+} removal from aqueous systems. However, Jin et al. (2018) and Xu et al. (2014) found that compared with plant straw-derived biochars, animal manure-derived biochars had larger sorption capacity for heavy metals. This inconsistency may be attributed to the following reasons: (i) the different contents or components of minerals in the feedstocks of studied biochars, which was supported by the result of Cantrell et al. (2012) that biochar properties across manure varieties varied under similar controlled conditions; and (ii) the acidification treatment of biochars, which removed minerals from biochars and reduced the contribution of precipitation mechanism to Cd^{2+} adsorption (Cui et al. 2016; Liu and Fan 2018; Zhang et al. 2015). As exhibited in Fig. 1b, the Cd^{2+} adsorption capacity of ARB decreased much than ASB. These results indicate that the mechanism of Cd^{2+} adsorption onto biochars may vary with both pyrolysis temperature and feedstock, and thus need further investigation.

Many kinds of adsorbents have been reported to remove Cd^{2+} from aqueous solution through adsorption (Table 2). Although, it is difficult to make comparisons as adsorption capacities are measured under specific experimental conditions including temperature, solution pH, metal ion concentration, dosage, particle size, competitive ions, and adsorbent properties (Deng et al. 2017; Mahdi et al. 2018), the results suggest that rice straw biochars have relatively high Cd^{2+} adsorption potential, in the top one third among other adsorbents reported in the literature (Table 2).

Cd^{2+} adsorption and desorption on RB700 and SB700

Adsorption isotherm

The isotherms for the adsorption of Cd^{2+} on SB700 and RB700 are exhibited in Fig. 2a and the parameters fitted by the Langmuir and Freundlich models are presented in Table 3. The adsorption data for RB700 and SB700 were better fitted by Freundlich model, with R^2_{adj} (adjusted coefficients of determination) values ranging between 0.953 and 0.959. Based on the Freundlich model, the nonlinearity n values for RB700 and SB700 were less than 1.0, suggesting that there was a great heterogeneity of Cd^{2+} sorption affinity by the biochars (Kim et al. 2013). The lower n values for RB700 implied that rice straw-derived biochars were more heterogeneous than swine manure-derived biochars. According to the Langmuir model, the values of maximum adsorption capacity (Q_m) for RB700 and SB700 were 66.24 and 46.50 mg g^{-1} (Table 3), respectively, which are similar to or higher than those of biochars produced from other biomass, such as wheat straw
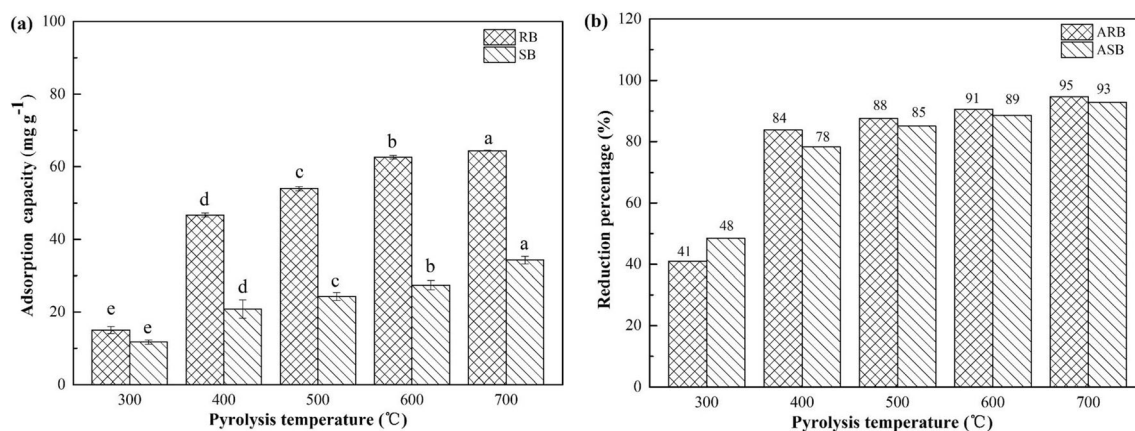
Fig. 1 Adsorption capacities for Cd^{2+} ($C_0 = 100$ mg L^{-1}) on rice straw and swine manure biochars produced at 300–700 °C (**a**); reduction percentages of Cd^{2+} adsorption capacities of RB and SB produced at 300–700 °C after acidification (**b**)

(38.4–69.8 mg g^{-1}) (Liu and Fan 2018) and municipal sewage sludge (18.80 mg g^{-1}) (Chen et al. 2014) (Table 2). Based on the classification system of Giles et al. (1974), the adsorption isotherms for Cd^{2+} on RB700 and SB700 are type L-1. Sposito (1989) reported that a type L-1 isotherm indicates a relatively high affinity of the sorbent for the sorbate. Therefore, the results demonstrated the potential of rice straw and swine manure biochars to be effective adsorbents for Cd^{2+} removal.

Distribution coefficient (K_d) is an index of the potential mobility of metals. A metal with a higher K_d value is characterized by stronger sorption onto biochar and thus lower solubility (Park et al. 2016). To compare the adsorption capacity of biochars, the distribution coefficients K_d ($K_d = Q_e/C_e$, L g^{-1}) calculated at different Cd^{2+} concentrations (10, 100, and 400 mg L^{-1}) were listed in Table 3. The values of K_d for RB700 and SB700 greatly decreased with increasing Cd^{2+} concentration, which could be explained by the nonlinearity of Cd^{2+} sorption on the biochars (Fig. 2a). The greater K_d values of RB700 than those of SB700 at any specific Cd^{2+} concentrations indicated that RB700 had stronger adsorption affinity for Cd^{2+}. On the other hand, the differences between K_d values of RB700 and SB700 declined with Cd^{2+} concentrations, showing the influence of initial Cd^{2+} concentrations on the adsorption capacity of biochars.

Adsorption kinetics

The adsorption kinetic results of Cd^{2+} on RB700 and SB700 are presented in Fig. 2b and the parameters fitted by kinetic models are presented in Table 4 and Table S1.

The PSO model was a better fit than the PFO model for the adsorption kinetics of Cd^{2+} on RB700 and SB700 with R^2_{adj} values between 0.974 and 0.991 (Table 4). In addition, the calculated Q_e values obtained from the PSO model were similar to the experimental Q_e. However, the successful description of experimental adsorption kinetic data by the PSO model

does not reveal the adsorption mechanisms (Tran et al. 2017). On the other hand, the importance of chemisorption can be evaluated by the Elovich model, which reflects a heterogeneous diffusion process controlled by the reaction rate and diffusion factor (Liu and Fan 2018). In this study, Cd adsorption was well described by Elovich model, with adjusted correlation coefficients (R^2_{adj}) between 0.969 and 0.977, indicating that chemical adsorption was the dominant adsorption process.

From Fig. 2b, it is evident that Cd^{2+} adsorption on both RB700 and SB700 increased rapidly during the first 12 h, increased slowly for the next 36 h, and reached equilibrium by 48 h. For example, Cd^{2+} amounts absorbed onto RB700 and SB700 after 12 h were 90.6% and 94.3% of the total Cd^{2+} adsorption amounts, respectively, while the Cd^{2+} adsorption amounts during the next 36 h only accounted for 9.4% and 5.7% of total adsorption, respectively. This indicated that the process of Cd^{2+} adsorption onto biochars consisted of fast and slow stages, which were supported by the fitting results of TC model with the adjusted coefficients (R^2_{adj}) > 0.98 (Table 4). The F_{fast} value (0.853) of SB700 was much larger than the F_{slow} value (0.147), implying that the fast adsorption stage was outstanding during the Cd^{2+} adsorption process of SB700, while that of RB700 was the opposite. The Cd^{2+} adsorption kinetics of sphagnum peat moss biochars showed a similar pattern (Ho and Mckay 1998; Lee et al. 2015). For RB700, the k_{fast} value was higher, thus the interaction between Cd^{2+} and the adsorption sites was very active, but not for SB700. This could be explained by the reason that precipitation with minerals contributed largely to Cd^{2+} adsorption and thus the adsorption rate is affected by the solubility of minerals in biochars (Liu and Fan 2018; Wang et al. 2015); however, more crystallized minerals were observed in SB700 compared with RB700 (Fig. S4).

The intraparticle diffusion (IPD) model can help determine the process and mechanisms of adsorption and evaluate the rate-controlling stages (Tran et al. 2017). It was proposed that

Table 2 Comparison of maximum Cd^{2+} adsorption capacities (Q_m) of different adsorbents reported in literature

Adsorbent	Pyrolysis temperature (°C)	Initial pH	Adsorbent (g): solution (mL)	Q_m (mg g^{-1})	References
Vanadium mine tailing	–	5.2	1:250	8.8	Shi et al. (2009)
Black gram husk	–	2–7	1:100	40.0	Saeed et al. (2005)
Pine sawdust biochar	200	5.0	1:1000	4.6	Peng et al. (2017)
	500			1.9	
	650			5.2	
Sesame straw biochar	700	7.0	1:500	86.0	Park et al. (2016)
Peat moss	–	5.0	1:1000	35.8	Lee et al. (2015)
Peat moss biochar	800			39.8	
Barley straw biochar	300	6.0	1:1000	1.6	Jazini et al. (2018)
	500			1.8	
Water hyacinth biochar	250	5.5	1:200	49.5	Zhang et al. (2015)
	450			70.3	
	550			34.0	
Municipal sewage sludge biochar	500	6.0	1:800	4.6	Chen et al. (2014)
	900			18.8	
Orange peel biochar	400	7.0	1:500	105.0	Tran et al. (2016)
	600			112.0	
	800			98.6	
Canna indica biochar	300	5.0	1:1000	63.3	Cui et al. (2016)
	500			188.8	
	600			140.0	
Wheat straw biochar	300	5.0	1:1000	38.4	Liu and Fan (2018)
	500			52.1	
	700			69.8	
Swine solids biochar	250	4.5	Not given	81.1	Han et al. (2017)
	600			31.9	
Poultry litter biochar	250			55.9	
	600			31.2	
Rice straw biochar	700	5.5	1:1000	66.2	This study
Swine manure biochar	700			46.5	

the adsorbate transfer process in a solid-liquid sorption system can be divided into the following steps: film diffusion or external diffusion, surface diffusion, and pore diffusion (Liu and Fan 2018; Tran et al. 2017). In this study, the data of Cd^{2+} sorption on RB700 and SB700 within 12 h was well fit by the IPD model (Table S1, Fig. 2b), proving that the intraparticle diffusion played a significant role in Cd^{2+} sorption. The values of intercept b, which can reflect the thickness of the boundary layer of the adsorbent (Kołodyńska et al. 2012; Tran et al. 2017; Wang et al. 2015), were 0.70 and 9.65 mg g^{-1} (larger than 0) for RB700 and SB700, respectively. This indicated that the transport process of Cd^{2+} from solution to biochar particle through the boundary layer may influence its adsorption kinetic process. Similarly, the Cd^{2+} adsorption process of RB700 and SB700 was controlled by a multistep mechanism according to the multiple linear regression plotted by the intraparticle diffusion model (Tran et al. 2017). The adsorption kinetic results show that chemical reactions dominated

Cd^{2+} adsorption on biochars, the biochars studied were heterogeneous, and the adsorption sites were distributed on the external and intraparticle biochar surfaces (Fig. 3).

Desorption characteristics

After Cd^{2+} had been equilibrated with the biochars at 25 °C for 24 h, the solution was removed, and 20 mL of 0.005 mol L^{-1} CaCl$_2$ was added to the biochar to facilitate desorption. The amount of Cd^{2+} desorbed from RB700 and SB700 as a function of contact time is shown in Fig. S5. The processes of Cd^{2+} desorption from RB700 and SB700 were similar and can be clearly divided into three phases: (1) a rapid initial rise in Cd^{2+} desorbed, (2) a slow decrease in the amount of Cd^{2+} desorbed, and (3) stable phase. Desorption of Cd^{2+} from SB700 reached the stable phase before RB700. Although the amounts of Cd^{2+} desorbed from RB700 were slightly larger than those of SB700, the Cd^{2+} removal
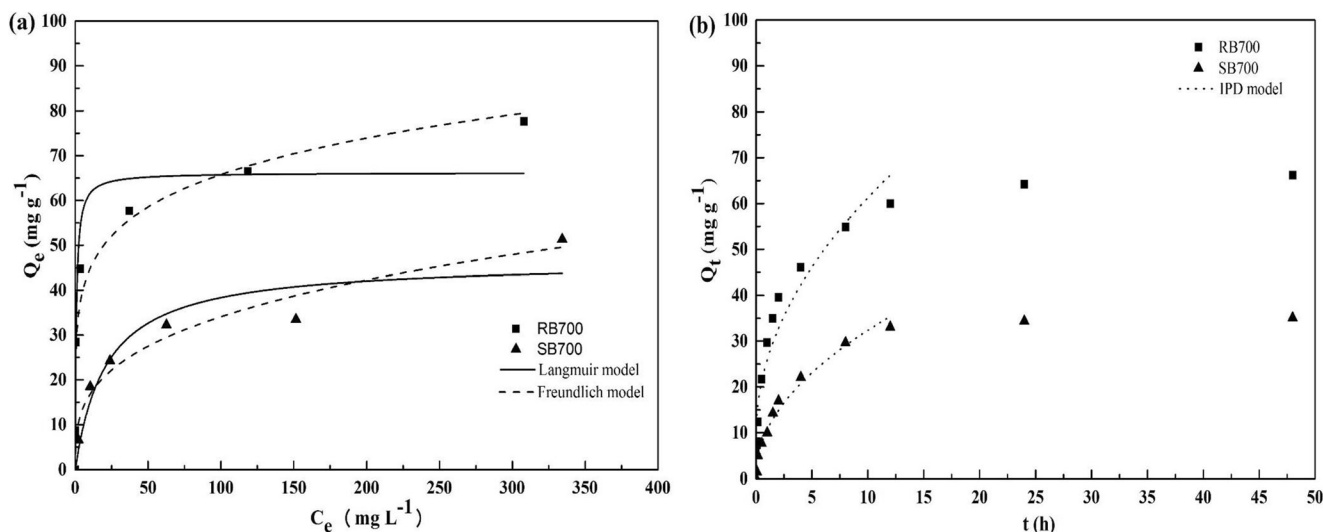
Fig. 2 Adsorption isotherms (**a**) and adsorption kinetics (**b**) of Cd^{2+} by RB700 and SB700. Q_e is the amount of Cd^{2+} absorbed on the sorbent (mg g^{-1}), C_e is the concentration of Cd^{2+} in solution at equilibrium; Q_t is the amount of Cd^{2+} adsorbed at time t (mg g^{-1}), the initial concentration of Cd^{2+} for adsorption kinetics is 100 mg L^{-1}, and the intraparticle diffusion (IPD) model fits the data before 12 h of Cd^{2+} sorption

efficiency of SB700 was higher than that of RB700 due to the much higher Cd^{2+} adsorption capacity of RB700 relative to SB700 (Cd^{2+} removal efficiency = amounts of Cd^{2+} desorbed/ amounts of Cd^{2+} adsorbed). This result indicated that rice straw biochar was more effective for immobilizing Cd^{2+} than swine manure biochar.

Electrostatically adsorbed ions are easily desorbed in an unbuffered neutral salt solution (Xu et al. 2005). For example, Jiang et al. (2014) proposed that the amount of Pb desorbed in 1.0 mol L^{-1} NaNO$_3$ was approximately equal to the amount of Pb electrostatically adsorbed onto soil and that both electrostatic and non-electrostatic adsorption mechanisms contributed to the binding of Pb by variably charged soils containing biochar. In this study (Fig. S5), phase 1, the rapid initial desorption of Cd^{2+} from the biochars, suggests that approximately 6 and 8 mg g^{-1} of Cd^{2+} were retained on the SB700 and RB700 by electrostatic interactions. Phase 2, the slow decrease in desorption of Cd^{2+} from the biochars, suggests

that once in the aqueous phase, the Cd^{2+} was re-adsorbed by a slow non-electrostatic reaction. Phase 3 indicates that eventually a new equilibrium was reached, conditioned by the 0.005 mol L^{-1} CaCl$_2$ background solution. Therefore, the small amounts desorbed from RB700 and SB700 by 0.005 mol L^{-1} CaCl$_2$ suggested that electrostatic interactions occurred between Cd^{2+} and the biochars but were not predominant.

Quantitative mechanisms of Cd^{2+} adsorption on the biochar

Cation exchange

Metal ions (Ca^{2+}, Mg^{2+}, K$^+$, and Na$^+$) are retained on biochar surfaces by electrostatic attraction to carboxylate groups, or phenol groups at higher pH values. During the adsorption process, Cd^{2+} in solution may be retained on the biochar by

Table 3 Langmuir and Freundlich isotherm (LM and FM) parameters for Cd^{2+} adsorption on RB700 and SB700

Biochar	LM						FM					
	Q_m $^\alpha$ (mg g^{-1})	K_L (L mg^{-1})	R^2_{adj} $^\beta$	K_d (L g^{-1}) $^\gamma$			K_F (mg g^{-1}) (mg L^{-1})$^{-1/n}$	n	R^2_{adj}	K_d (L g^{-1})		
				10	100	400				10	100	400
RB700	66.235	1.305	0.929	6.152	0.657	0.165	30.322	0.168	0.953	4.464	0.657	0.207
SB700	46.500	0.047	0.912	1.487	0.383	0.110	8.204	0.310	0.959	1.675	0.342	0.131

$^\alpha$ Q_m is the maximum adsorption capacity of LM, mg g^{-1}

$^\beta$ R^2_{adj} is the adjusted coefficient of determination and it is influenced by both the number of data points (m) and the number of fitting parameters (p), $R^2_{adj} = 1 - (m-1)(1-R^2)/(m-p-1)$

$^\gamma$ K_d values were calculated at different equilibrium concentrations of Cd^{2+} (10, 100, and 400 mg L^{-1}), L g^{-1}. $K_d = Q_e/C_e$. Q_e was determined by models (LM and FM)

Table 4 The fitting results of Cd^{2+} adsorption kinetics on RB700 and SB700 using pseudo-second-order (PSO) model and two-compartment (TC) model

Biochar	Q_e (exp) [α] (mg g^{-1})	PSO model			TC model					
		k_2 (g mg^{-1} h^{-1})	Q_e (cal) [β] (mg g^{-1})	R^2_{adj}	Q_e (cal) (mg g^{-1})	F_{fast}	F_{slow}	k_{fast} (h^{-1})	k_{slow} (h^{-1})	R^2_{adj}
RB700	64.40	0.0162	65.49	0.974	65.41	0.408	0.592	2.818	0.169	0.983
SB700	34.20	0.0084	33.76	0.991	34.83	0.853	0.147	0.226	5.521	0.996

[α] Q_e (exp) is the amount of Cd^{2+} sorption at equilibrium from the experimental results, mg g^{-1}

[β] Q_e (cal) is the adsorption capacity at equilibrium calculated by kinetic model, mg g^{-1}

cation exchange reactions with these metals (Cui et al. 2016; Lu et al. 2012). To quantify the amount of Cd^{2+} retained by cation exchange, we calculated the net release of metals ions (Ca^{2+}, Mg^{2+}, K^+ and Na^+) in the solution with and without Cd^{2+} sorption (blank samples). The amount of metal cations released during Cd^{2+} sorption was greater for low-temperature (400 °C) than high-temperature (700 °C) biochars (Table 5). Accordingly, the amount of Cd^{2+} adsorbed via cation exchange was much larger on biochars produced at 400 °C than that at 700 °C. This is attributed to decarboxylation, which primarily occurs at high temperatures, and results in the loss of negatively charged carboxylate groups and, hence, lower CEC in high-temperature relative to low-temperature biochars (Keiluweit et al. 2010; Lawrinenko and Laird 2015; Wang et al. 2015).

Precipitation with minerals

Many inorganic minerals contributed to the ash phase in the biochars and the ash content increased with pyrolysis temperature (Table 1, Fig. S4). Previous studies have reported that precipitation of Cd^{2+} forming various mineral phases can contribute to Cd^{2+} adsorption (Cui et al. 2016; Zhang et al. 2015). As shown in Fig. 1b, remarkable decreases in Cd^{2+} adsorption capacity were observed when biochars (RB and SB) were demineralized by acidification. With increasing pyrolysis temperature, the reduction percentage of Cd^{2+} adsorption capacities of RB and SB increased from approximately 40 to 90%, suggesting that precipitation of Cd^{2+} as minerals played a more significant role in high-temperature biochars than in low-temperature biochars. Cd^{2+} can be precipitated with CO_3^{2-}, PO_4^{3-}, and OH^- released from biochars. However, the critical pH value for the formation of Cd $(OH)_2$ (K_{sp}= 7.2×10^{-15}, 25 °C) at a Cd^{2+} concentration of 100 mg L^{-1} was approximately 7.5, which was higher than the pH values (between 6.34 and 7.13) of solutions after reaching Cd^{2+} adsorption equilibrium in this study (Fig. 5a); thus, the formation of Cd $(OH)_2$ may not account for the Cd^{2+} precipitates in biochars.

SEM-EDS analyses were conducted to further investigate the mechanisms of Cd adsorption. Relative to the original biochar, many white granular crystals dispersed on the surfaces of Cd-loaded biochars, and EDS analysis confirmed that these white granular crystals contained Cd (Fig. 3). Furthermore, the atom % Cd^{2+} for the surface sites analyzed by EDS were much higher for the Cd-loaded rice straw-derived biochars (RB400 and RB700) than for the Cd-loaded swine manure-derived biochars (SB400 and SB700), and that the atom % Cd^{2+} for high-temperature biochars (700 °C) were higher than for low-temperature biochars (400 °C). The high concentrations of Cd in the white granular crystals evident in the SEM-EDS data for the Cd-loaded 700 °C biochars are consistent with the precipitation of Cd mineral phases.

XRD analysis was conducted to identify the crystalline mineral phases present in the biochars. The XRD results clearly identified $CdCO_3$ phases in the Cd-loaded RB400 and Cd-loaded RB700 samples (Fig. 4), indicating that the Cd-rich white granular precipitates identified by SEM-EDS (Fig. 3) were $CdCO_3$. By contrast, no Cd mineral phases were found in the XRD patterns of the Cd-loaded swine manure-biochars (Fig. 4) although white precipitates containing Cd were identified by SEM-EDS (Fig. 3). These results suggest that Cd^{2+} formed amorphous precipitates (possibly with $Cd_3(PO_4)_2$) or that the concentration of crystalline phases was too low to be detected by XRD (Cao et al. 2009).

Complexation with oxygen-containing functional groups

Complexation of metals with surface oxygen-containing functional groups (e.g., –COOH, –OH, −R–OH) through cation exchange has been reported to be an important mechanism for metal adsorption by biochar (Cui et al. 2016). Other researchers have confirmed the impacts of inner sphere surface complexation with oxygen-containing groups in Cd^{2+} adsorption by qualifying the Cd-loaded biochars by FTIR and XPS (Cui et al. 2016; Zhang et al. 2015). Moreover, the release of H^+ was reported to be accompanying complexation with surface oxygen-containing groups (Cao et al. 2009; Cui et al. 2016), resulting in a decrease of solution pH values. In this study, with an initial pH of 5.5, however, the solution pH values increased after Cd^{2+} sorption on biochars (Fig. 5a), which could be caused by the dissolution of minerals in the
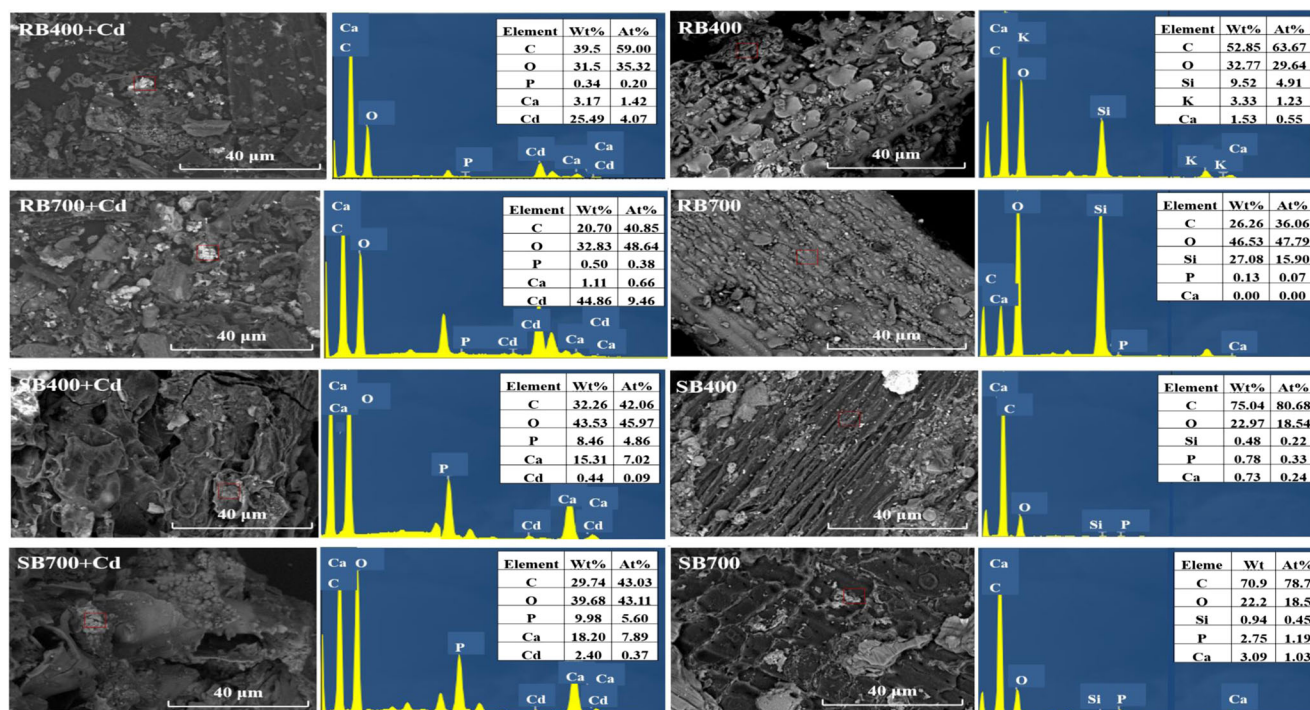
Fig. 3 SEM images (left) and corresponding EDS spectra (right) of RB and SB before (RB, SB) and after (RB+Cd, SB+Cd) reaction with cadmium

biochars (Wang et al. 2015). Therefore, in order to exclude the effect of mineral ash on solution pH, biochars were demineralized by acidification (Section "Production of biochars"); and a Cd^{2+} adsorption experiment was performed with acidified biochars (ARB and ASB). With the acidified biochars, a decrease in pH values (pH_D) after Cd^{2+} adsorption was observed (Fig. 5b). In addition, the mechanism of complexation with functional groups was also supported by the positive correlation between pH_D values and the polarity index ((O+N)/C) for the biochars ($R^2 = 0.93$, 0.98 for ARB and ASB, respectively, $p < 0.05$, Fig. S6a).

Thus, Cd-π interactions could occur on the surface of biochars, particularly on the highly aromatic surfaces of high-temperature biochars (Xu et al. 2014). Harvey et al. (2011) reported that cation-π interactions are the predominant Cd^{2+} adsorption mechanism for plant-derived biochars with low polarity. Cui et al. (2016) reported that in Cd-loaded biochars, an obvious shift observed for FTIR peaks attributed to aromatic C-H at 832 and 704 cm^{-1} in the high-temperature biochars and -CH$_2$- at 1402 cm^{-1}, while the C=C stretching peak (1626 cm^{-1}) exhibited a redshift and expanding width. Such evidence suggests that Cd^{2+}-π interactions may contribute to Cd^{2+} adsorption.

Cation-π interactions

Aromatic carbon compounds on biochar surfaces are electron-rich π-systems that may donate π-electrons to interact with Cd^{2+}, which could act as a π-acceptor due to its electron deficiency.

Quantitative contributions of mechanisms

Based on the method discussed in Section "Quantitative contributions of Cd2+ adsorption mechanisms," we estimate the contribution of cation exchange with metals (Q_{ci}),

Table 5 Major cations released from and Cd^{2+} adsorbed onto biochars during Cd^{2+} adsorption

Elements (mEq L^{-1})	The net amount of metal cations released [α]							Total Cd^{2+} adsorbed
	K	Ca	Na	Mg	Monovalent	Divalent	Sum	
RB400	0.060	0.259	0.026	0.079	0.086	0.338	0.423	0.831
RB700	0.012	0.137	0.052	0.048	0.064	0.185	0.249	1.146
SB400	0.022	0.012	0.065	0.060	0.087	0.072	0.160	0.371
SB700	0.006	0.084	0.012	0.022	0.018	0.106	0.124	0.610

[α] The net amount of metal cations released was calculated by subtracting the metals' amounts of blank sample (biochar added in background solution) from that of the corresponding experimental group (biochar added in Cd^{2+} solution)
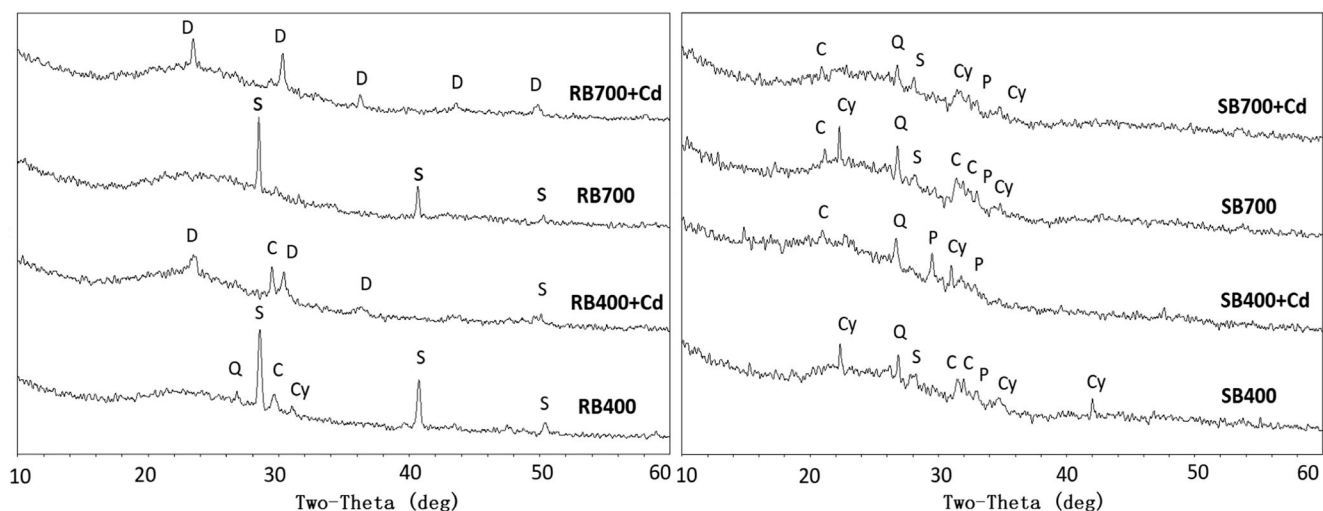
Fig. 4 XRD patterns of biochars before (RB, SB) and after (RB+Cd, SB+Cd) reaction with cadmium. Minerals with peaks labeled: Q, quartz; S, Sylvite; C, calcite; D, $CdCO_3$; Cy, calcium silicate; and P, calcium phosphate

precipitation with minerals (Q_{cp}), complexation with oxygen-containing functional groups (Q_{co}), and Cd^{2+}-π interactions ($Q_{c\pi}$) to the total Cd^{2+} adsorption capacities of RB and SB produced at 400 and 700 °C (Fig. 6 and Table S2). With increasing pyrolysis temperature, from 400 to 700 °C, the values of Q_{ci} (Fig. 6a) and Q_{ci}/Q_c (Fig. 6b) decreased. For example, the Q_{ci} and Q_{ci}/Q_c values of RB400 were 23.79 mg g^{-1} and 50.90%, which were larger than those values of RB700 with 14.00 mg g^{-1} and 21.74%. Moreover, the Q_{ci} and Q_{ci}/Q_c values of RB were larger than those of SB at either 400 or 700 °C (Table S2). Conversely, the contribution percentage of precipitation with minerals to Cd^{2+} adsorption (Q_{cp}/Q_c) by RB and SB increased with pyrolysis temperature, from 32.91 and 34.99% at 400 °C to 72.93 and 72.49% at 700 °C, respectively. Compared with those of high-temperature biochars (700 °C), the Q_{co} (Fig. 6a) and Q_{co}/Q_c (Fig. 6b) values of low-temperature biochars (400 °C) were

much larger. For instance, the values of Q_{co} and Q_{co}/Q_c of SB400 were 3.91 mg g^{-1} and 18.78%, which were approximately 9 and 17 times than those for SB700, respectively. This finding is attributed to the decrease in oxygen-containing functional groups in high-temperature biochars relative to those in low-temperature biochars, which is supported by the negative correlation between the Q_{co} values and polarity ((O+N)/C) of biochars (Fig. S6b). For biochars produced at 400 °C, the Q_{cp} and Q_{co} values of RB400 were larger than those of SB400, but the Q_{cp}/Q_c and Q_{co}/Q_c values of SB400 were larger than RB400. This finding implied that precipitation and complexation in SB were more important than those in RB to overall Cd^{2+} adsorption. The contribution of coordination with π electrons ($Q_{c\pi}$ and $Q_{c\pi}/Q_c$) to the Cd^{2+} adsorption by the biochars increased with increasing pyrolysis temperature from 400 to 700 °C. For example, the $Q_{c\pi}$ value of RB400 was only 0.66 mg g^{-1}, while the $Q_{c\pi}$ value of RB700 was
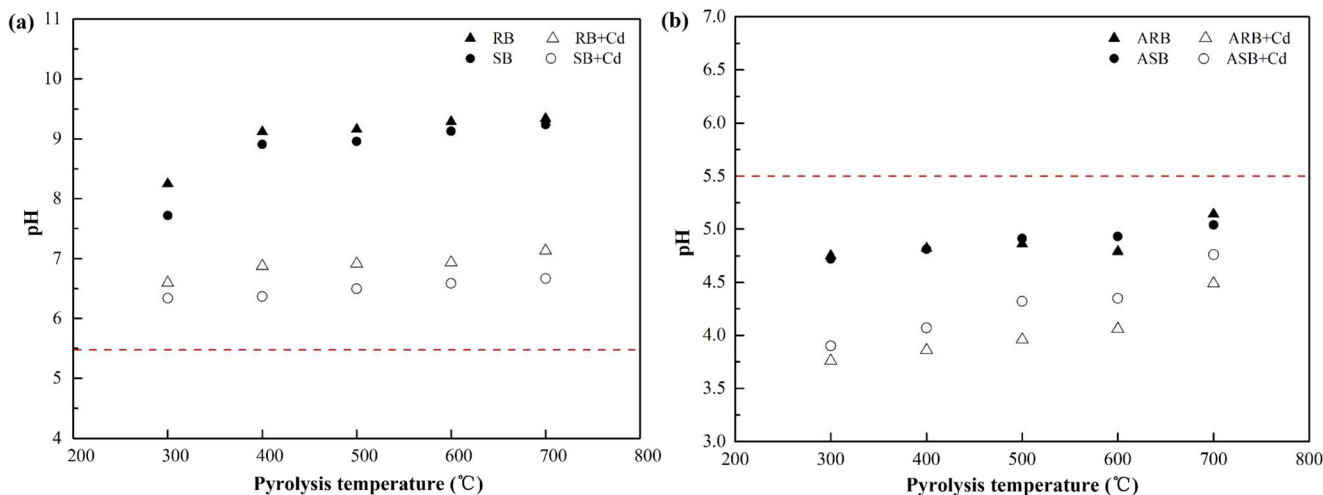

Fig. 5 The pH values of the mixed solution of RB, SB, ARB, and ASB with and without Cd^{2+} after equilibration shaking 24 h (initial Cd^{2+} concentration was 100 mg L^{-1}); the initial pH of all solutions was 5.5 ± 0.1
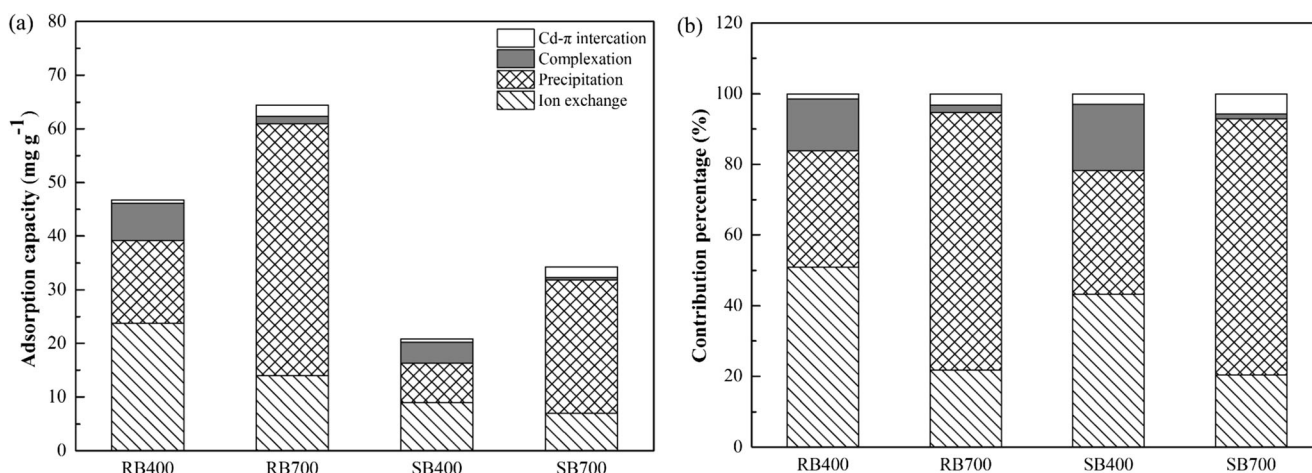
Fig. 6 The estimated contribution to Cd^{2+} adsorption attributed to cation exchange with metals (Q_{ci}), precipitation with minerals (Q_{cp}), surface complexation with oxygen-containing functional groups (Q_{co}) and Cd^{2+}–π interactions ($Q_{c\pi}$) on RB and SB produced at 400 and 700 °C

2.02 mg g^{-1} (Fig. 6a, Table S2). Moreover, for the same pyrolysis temperature, the $Q_{c\pi}$ values for RB were larger than those for SB (Fig. 6a), indicating that more aromatic structures were formed in RB than those in SB at a given temperature. The significant negative correlation between $Q_{c\pi}$ and the aromaticity (H/C) of biochars further confirmed the coordination of Cd^{2+} with π electrons on the biochars ($R^2 = 0.97$, 0.96 for RB and SB, respectively, $p < 0.01$, Fig. S7). These results revealed that all the mechanisms (precipitation, complexation, cation exchange, and Cd^{2+}-π interactions) contributed to the different Cd^{2+} adsorption capacities of biochars derived from rice straw and swine manure, but precipitation and ion exchange were prominent; cation exchange was the dominant mechanism of Cd^{2+} adsorption on biochars produced at a low temperature (400 °C) (accounting for 43.3–50.9%), while precipitation with minerals accounting for approximately 72% of Cd^{2+} adsorption by biochars produced at a high temperature (700 °C).

Conclusions

Biochars produced from plant residual (rice straw) and animal waste (swine manure) at different temperatures (i.e., 300, 400, 500, 600, and 700 °C) exhibited dissimilar characteristics (properties, surface characteristics, and Cd^{2+} adsorption capacities). The most effective pyrolysis temperature for Cd^{2+} adsorption onto rice straw- and swine manure-biochars was 700 °C, and RB700 was the most efficient biochar with a maximum Cd^{2+} adsorption capacity of 64.4 mg g^{-1} and desorption capacity of 3.65 mg g^{-1}. The adsorption and kinetics results revealed that chemical reactions dominated Cd^{2+} adsorption on biochars, sorption includes both fast and slow adsorption processes, and the Cd^{2+} adsorption rate was controlled by film and intraparticle diffusion. Adsorption of Cd^{2+} on biochars involved the following mechanisms: (i)

precipitation with minerals, (ii) cation exchange, (iii) complexation with surface oxygen-containing functional groups, and (iv) cation-π interactions. In general, cation exchange was the dominant mechanism of Cd^{2+} adsorption by biochars prepared at a low temperature (400 °C) (accounting for 43.3–50.9%), while precipitation with minerals controlled Cd^{2+} adsorption by biochars produced at a high temperature (700 °C) (accounting for approximately 72%). All of these mechanisms contributed to the difference in Cd^{2+} adsorption capacity between rice straw- and swine manure-derived biochars, but precipitation and ion exchange were prominent. The results from this study suggested that biochar derived from rice straw is a promising adsorbent for the Cd^{2+} removal from wastewater and that the low-temperature biochar may outperform the high-temperature biochar for Cd^{2+} immobilization in acidic water or soil. A novel contribution of this work is quantifying the impacts of pyrolysis temperature on mechanisms of Cd^{2+} adsorption for two important biomass feedstocks that are used for biochar production. Understanding the adsorption mechanism will help biochar manufacturers to optimize their products for Cd adsorption in different types of soils.

References

Ahmad M, Rajapaksha AU, Lim JE, Zhang M, Bolan N, Mohan D, Vithanage M, Lee SS, Ok YS (2014) Biochar as a sorbent for contaminant management in soil and water: a review. Chemosphere 99: 19–33

Ali I, Gupta VK (2007) Advances in water treatment by adsorption technology. Nat Protoc 1:2661–2667

Banik C, Lawrinenko M, Bakshi S, Laird DA (2018) Impact of pyrolysis temperature and feedstock on surface charge and functional group chemistry of biochars. J Environ Qual 47:452–461

Bashir S, Zhu J, Fu Q, Hu H (2018) Comparing the adsorption mechanism of Cd by rice straw pristine and KOH-modified biochar. Environ Sci Pollut Res Int 25:11875–11883

Beesley L, Morenojimenez E, Gomezeyles JL, Harris E, Robinson B, Sizmur T (2011) A review of biochars' potential role in the remediation, revegetation and restoration of contaminated soils. Environ Pollut 159:3269–3282

Cantrell KB, Hunt PG, Uchimiya M, Novak JM, Ro KS (2012) Impact of pyrolysis temperature and manure source on physicochemical characteristics of biochar. Bioresour Technol 107:419–428

Cao X, Harris W (2010) Properties of dairy-manure-derived biochar pertinent to its potential use in remediation. Bioresour Technol 101:5222–5228

Cao X, Ma L, Gao B, Harris W (2009) Dairy-manure derived biochar effectively sorbs lead and atrazine. Environ Sci Technol 43:3285–3291

Chen B, Zhou D, Zhu L (2008) Transitional adsorption and partition of nonpolar and polar aromatic contaminants by biochars of pine needles with different pyrolytic temperatures. Environ Sci Technol 42:5137–5143

Chen T, Zhang Y, Wang H, Lu W, Zhou Z, Ren L (2014) Influence of pyrolysis temperature on characteristics and heavy metal adsorptive performance of biochar derived from municipal sewage sludge. Bioresour Technol 164:47–54

Chen Z, Liu T, Tang J, Zheng Z, Wang H, Shao Q, Chen G, Li Z, Chen Y, Zhu J, Feng T (2018) Characteristics and mechanisms of cadmium adsorption from aqueous solution using lotus seedpod-derived biochar at two pyrolytic temperatures. Environ Sci Pollut Res 25:11854–11866

Cui X, Fang S, Yao Y, Li T, Ni Q, Yang X, He Z (2016) Potential mechanisms of cadmium removal from aqueous solution by Canna indica derived biochar. Sci Total Environ 562:517–525

Deng J, Liu Y, Liu S, Zeng G, Tan X, Huang B, Tang X, Wang S, Hua Q, Yan Z (2017) Competitive adsorption of Pb (II), Cd (II) and Cu (II) onto chitosan-pyromellitic dianhydride modified biochar. J Colloid Interface Sci 506:355–364

Fidel RB, Laird DA, Thompson ML, Lawrinenko M (2017) Characterization and quantification of biochar alkalinity. Chemosphere 167:367–373

Giles CH, Smith D, Huitson A (1974) A general treatment and classification of the solute adsorption isotherm. I. Theoretical. J Colloid Interface Sci 47(3):755–765

Han L, Sun H, Ro KS, Sun K, Libra JA, Xing B (2017) Removal of antimony (III) and cadmium (II) from aqueous solution using animal manure-derived hydrochars and pyrochars. Bioresour Technol 234:77–85

Harvey OR, Herbert BE, Rhue RD, Kuo L (2011) Metal interactions at the biochar-water interface: energetics and structure-sorption relationships elucidated by flow adsorption microcalorimetry. Environ Sci Technol 45:5550–5556

Higashikawa FS, Conz RF, Colzato M, Cerri CEP, Alleoni LRF (2016) Effects of feedstock type and slow pyrolysis temperature in the production of biochars on the removal of cadmium and nickel from water. J Clean Prod 137:965–972

Ho YS, Mckay G (1998) A comparison of chemisorption kinetic models applied to pollutant removal on various sorbent. Process Saf Environ Prot 76:332–340

Jazini R, Soleimani M, Mirghaffari N (2018) Characterization of barley straw biochar produced in various temperatures and its effect on lead and cadmium removal from aqueous solutions. Water Environ J 32:125–133

Jiang TY, Xu RK, Gu TX, Jiang J (2014) Effect of crop-straw derived biochars on Pb (II) adsorption in two variable charge soils. J Integr Agric 13:507–516

Jin J, Li S, Peng X, Liu W, Zhang C, Yang Y, Han L, Du Z, Sun K, Wang X (2018) HNO3 modified biochars for uranium (VI) removal from aqueous solution. Bioresour Technol 256:247–253

Keiluweit PSN, Mark GJ, Kleber M (2010) Dynamic molecular structure of plant biomass-derived black carbon (biochar). J Environ Chem Eng 44:1247–1253

Kim WK, Shim T, Kim YS, Hyun S, Ryu C, Park YK, Jung J (2013) Characterization of cadmium removal from aqueous solution by biochar produced from a giant Miscanthus at different pyrolytic temperatures. Bioresour Technol 138:266–270

Kołodyńska D, Wnętrzak R, Leahy JJ, Hayes MHB, Kwapiński W, Hubicki Z (2012) Kinetic and adsorptive characterization of biochar in metal ions removal. Chem Eng J 197:295–305

Lawrinenko M, Laird DA (2015) Anion exchange capacity of biochar. Green Chem 17:4628–4636

Lee SJ, Park JH, Ahn YT, Chung JW (2015) Comparison of heavy metal adsorption by peat moss and peat moss-derived biochar produced under different carbonization conditions. Water Air Soil Pollut 226:1–11

Li R, Liang W, Huang H, Jiang S, Guo D, Li M, Zhang Z, Ali A, Wang JJ (2018) Removal of cadmium (II) cations from an aqueous solution with aminothiourea chitosan strengthened magnetic biochar. J Appl Polym Sci 135:1–11

Liu L, Fan S (2018) Removal of cadmium in aqueous solution using wheat straw biochar: effect of minerals and mechanism. Environ Sci Pollut Res Int 25:8688–8700

Lu H, Zhang W, Yang Y, Huang X, Wang S, Qiu R (2012) Relative distribution of Pb^{2+} sorption mechanisms by sludge-derived biochar. Water Res 46:854–862

Ma Z, Yang Y, Ma Q, Zhou H, Luo X, Liu X, Wang S (2017) Evolution of the chemical composition, functional group, pore structure and crystallographic structure of bio-char from palm kernel shell pyrolysis under different temperatures. J Anal Appl Pyrolysis 127:350–359

Mahdi Z, Yu QJ, El Hanandeh A (2018) Investigation of the kinetics and mechanisms of nickel and copper ions adsorption from aqueous solutions by date seed derived biochar. J Environ Chem Eng 6:1171–1181

Meng J, Feng X, Dai Z, Liu X, Wu J, Xu J (2014) Adsorption characteristics of Cu (II) from aqueous solution onto biochar derived from swine manure. Environ Sci Pollut Res Int 21:7035–7046

Ministry of Environmental Protection, Ministry of Land and Resources (2014) The national survey of soil pollution. Available http://www.zhb.gov.cn/gkml/hbb/qt/201404/t20140417_270670.htm

Mohammadi N, Khani H, Gupta VK, Amereh E, Agarwal S (2011) Adsorption process of methyl orange dye onto mesoporous carbon material-kinetic and thermodynamic studies. J Colloid Interface Sci 362:457–462. https://doi.org/10.1016/j.jcis.2011.06.067

Pan J, Jiang J, Xu R (2013) Adsorption of Cr (III) from acidic solutions by crop straw derived biochars. J Environ Sci 25:1957–1965

Park JH, Ok YS, Kim SH, Cho JS, Heo JS, Delaune RD, Seo DC (2016) Competitive adsorption of heavy metals onto sesame straw biochar in aqueous solutions. Chemosphere 142:77–83

Peng H, Gao P, Chu G, Pan B, Peng J, Xing B (2017) Enhanced adsorption of Cu (II) and Cd (II) by phosphoric acid-modified biochars. Environ Pollut 229:846–853

Rafiq MT, Aziz R, Yang X, Xiao W, Rafiq MK, Ali B, Li T (2014) Cadmium phytoavailability to rice (Oryza sativa L.) grown in representative Chinese soils. A model to improve soil environmental quality guidelines for food safety. Ecotoxicol Environ Saf 103:101–107

Saeed A, Iqbal M, Akhtar MW (2005) Removal and recovery of lead (II) from single and multimetal (Cd, Cu, Ni, Zn) solutions by crop milling waste (black gram husk). J Hazard Mater 117:65–73

Shi T, Jia S, Chen Y, Wen Y, Du C, Guo H, Wang Z (2009) Adsorption of Pb (II), Cr (III), Cu (II), Cd (II) and Ni (II) onto a vanadium mine tailing from aqueous solution. J Hazard Mater 169:838–846

Shinogi Y, Kanri Y (2003) Pyrolysis of plant, animal and human waste: physical and chemical characterization of the pyrolytic products. Bioresour Technol 90:241–247

Sposito (1989) The chemistry of soils. Oxford University Press, New York (NY)

Tran HN, You SJ, Chao HP (2016) Effect of pyrolysis temperatures and times on the adsorption of cadmium onto orange peel derived biochar. Waste Manag Res 34:129–138

Tran HN, You SJ, Hosseini-Bandegharaei A, Chao HP (2017) Mistakes and inconsistencies regarding adsorption of contaminants from aqueous solutions: a critical review. Water Res 120:88–116

Uchimiya M, Lima IM, Klasson KT, Chang S, Wartelle LH, Rodgers JE (2010) Immobilization of heavy metal ions (CuII, CdII, NiII, and PbII) by broiler litter-derived biochars in water and soil. J Agric Food Chem 58:5538–5544

Uchimiya M, Wartelle LH, Klasson KT, Fortier CA, Lima IM (2011) Influence of pyrolysis temperature on biochar property and function as a heavy metal sorbent in soil. J Agric Food Chem 59:2501–2510

Wang Z, Liu G, Zheng H, Li F, Ngo HH, Guo W, Liu C, Chen L, Xing B (2015) Investigating the mechanisms of biochar's removal of lead from solution. Bioresour Technol 177:308–317

Wang Z, Shen F, Shen D, Jiang Y, Xiao R (2017) Immobilization of Cu(2+) and Cd(2+) by earthworm manure derived biochar in acidic circumstance. J Environ Sci (China) 53:293–300

Wang RZ, Huang DL, Liu YG, Zhang C, Lai C, Zeng GM, Cheng M, Gong XM, Wan J, Luo H (2018) Investigating the adsorption behavior and the relative distribution of Cd(2+) sorption mechanisms on biochars by different feedstock. Bioresour Technol 261:265–271

Xu R, Xiao S, Zhao A, Ji G (2005) Effect of Cr (VI) anions on adsorption and desorption behavior of Cu (II) in the colloidal systems of two authentic variable charge soils. J Colloid Interface Sci 284:22–29

Xu X, Cao X, Zhao L (2013a) Comparison of rice husk- and dairy manure-derived biochars for simultaneously removing heavy metals from aqueous solutions: role of mineral components in biochars. Chemosphere 92:955–961

Xu X, Cao X, Zhao L, Wang H, Yu H, Gao B (2013b) Removal of Cu, Zn, and Cd from aqueous solutions by the dairy manure-derived biochar. Environ Sci Pollut Res Int 20:358–368

Xu D, Zhao Y, Sun K, Gao B, Wang Z, Jin J, Zhang Z, Wang S, Yan Y, Liu X, Wu F (2014) Cadmium adsorption on plant- and manure-derived biochar and biochar-amended sandy soils: impact of bulk and surface properties. Chemosphere 111:320–326

Yuan JH, Xu RK, Zhang H (2011) The forms of alkalis in the biochar produced from crop residues at different temperatures. Bioresour Technol 102:3488–3497

Zhang W, Mao S, Chen H, Huang L, Qiu R (2013) Pb (II) and Cr (VI) sorption by biochars pyrolyzed from the municipal wastewater sludge under different heating conditions. Bioresour Technol 147: 545–552

Zhang F, Wang X, Yin D, Peng B, Tan C, Liu Y, Tan X, Wu S (2015) Efficiency and mechanisms of Cd removal from aqueous solution by biochar derived from water hyacinth (Eichornia crassipes). J Environ Manag 153:68–73